Supplement of The Cryosphere, 8, 1289–1296, 2014
http://www.the-cryosphere.net/8/1289/2014/
doi:10.5194/tc-8-1289-2014-supplement

The Cryosphere Open Access

Supplement of

A spurious jump in the satellite record: has Antarctic sea ice expansion been overestimated?

I. Eisenman et al.

Correspondence to: I. Eisenman (eisenman@ucsd.edu)

Supplemental Discussion and Figures

S1 Detailed description of data and methods

Here we discuss the ice concentration fields analyzed in this study and the resulting time series of ice extent and ice area that we calculate.

S1.1 Ice concentration

The ice concentration data sets considered in this study are derived from passive microwave measurements from instruments flown on a series of satellites. The Scanning Multichannel Microwave Radiometer (SMMR) was flown on the NASA Nimbus 7 satellite and provided data between 26 October 1978 and 20 August 1987, with the Bootstrap sea ice concentration using the data between 1 November 1978 and 31 July 1987. SSMR measured radiances in 10 channels including 18.0H, 18.0V, 21.0V, 37.0H, and 37.0V; here the number refers to the frequency in GHz and the letter indicates vertical (V) or horizontal (H) polarization. Although the Nimbus 7 passed over both polar regions every day, the radiometer operated only on alternate days due to power limitations, leading to a temporal resolution of 2 days. SMMR was succeeded by the Special Sensor Microwave/Imager (SSM/I), which measured radiances every day in 7 channels including 19.3H, 19.3V, 22.2V, 37.0H, and 37.0V. SSM/I instruments were flown on a sequence of three Defense Meteorological Satellite Program (DMSP) satellites beginning in July 1987. For the Bootstrap sea ice concentration, data from the DMSP F8 satellite is used from 1 August 1987 until 2 December 1991, data from the DMSP F11 satellite is used from 3 December 1991 until 30 September 1995, and data from the DMSP F13 satellite is used from 1 October 1995 to 31 December 2007. The sensor transition that we focus on in this study is between the F8 and F11 platforms in December 1991. The Special Sensor Microwave Imager Sounder (SSMIS), which measures radiances in 24 different channels including 19.3H, 19.3V, 22.2V, 37.0H, and 37.0V, has been generating daily data from a Department of Defense satellite since 14 December 2006, with the Bootstrap sea ice concentration using data starting on 1 January 2008.

We consider both hemispheres in this Supplement. We focus on ice concentration data sets generated from the passive microwave radiance measurements using the Bootstrap algorithm, and in this Supplement we also consider data generated with the NASA Team algorithm. The Bootstrap algorithm uses data from the 19V, 37V, and 37H channels, and the NASA Team algorithm uses data from the 19H, 19V, and 37V channels. Both algorithms also draw on the 22V channel to filter out weather effects. The use of brightness temperature ratios in the NASA Team algorithm reduces errors due to surface temperature variations, but unlike the Bootstrap algorithm, the NASA Team algorithm is biased toward underestimating sea ice concentrations (Comiso et al., 1997). Both algorithms have empirically adjusted parameters that differ between the two hemispheres, and the parameters in the Bootstrap algorithm also vary on a daily basis.

Various steps go into processing the ice concentration data to intercalibrate across the transition from one sensor to another and to fill in missing or identifiably erroneous pixels. Although a number of brief data gaps exist, the instruments have provided data for at least 20 days of every month (10 days for SMMR) from November 1978 to present with the exception of December 1987 and January 1988, when the SSM/I instrument was turned off between 3 December 1987 and 13 January 1988 due to overheating issues.

The effective resolution (sensor footprint) of the microwave measurements vary as a function of frequency, with the resolution of the most coarse frequency used by the Bootstrap and NASA Team algorithms being approximately 40 km $\times$ 70 km. However, all concentrations are derived from daily passive microwave brightness temperatures mapped onto a polar stereographic grid with a nominal resolution of 25 $\times$ 25 km.

A region around each pole is not imaged due to the inclination angle of the satellite orbit. This hole is located poleward of 84.5°N for SMMR and 87.2°N for SSM/I. SSMIS has a slightly smaller hole than SSM/I, but the SSM/I hole is used for SSMIS to simplify processing.

The Bootstrap data is processed at NASA Goddard Space Flight Center and distributed by the National Snow and Ice Data Center (NSIDC) (Comiso, 2000), and we acquired from NSIDC the daily Bootstrap ice concentration data sets from before (Version 1) and after (Version 2) the entire data set was reprocessed in September 2007 using an updated Bootstrap algorithm (see Sect S1.3).

S1.2 Ice extent and ice area

We calculate the daily ice area in a given hemisphere from the gridded ice concentration field in both Bootstrap versions by summing the surface area of all grid cells weighted by the ice concentration. Following a standard convention (e.g., Cavalieri et al., 1999), we exclude grid cells with ice concentration less than 15% due to wind roughening and other weather filtering issues near the ice edge.

A more common measure of the hemispheric sea ice cover is the ice extent, which is defined as the sum of the surface area of all pixels with ice concentration above a specified threshold, normally taken to be 15% since this has been found to correspond with the ice edge estimated using aircraft measurements (Cavalieri et al., 1991). In other words, the ice extent includes the area of leads within grid cells that have ice concentration above 15%, whereas the ice area does not. We calculate the daily ice extent for both Bootstrap versions following this convention, and ice extent is used exclusively in the main paper. An advantage of using ice extent rather than ice area is that ice extent is less sensitive to er-

rors in the ice concentration field, such as those associated with the misidentification of surface melt ponds during the summer as open ocean. Two disadvantages of using ice extent rather than ice area are that ice extent is less physically relevant, since it includes the area of patches of open water within the ice pack, and that ice extent depends more on pixel resolution.

In the Arctic, we mask lakes from the ice concentration field and assume the hole around the pole has 100% ice concentration; note that this causes a small erroneous decrease in Arctic sea ice area in 1987 associated with the decrease in the radius of the hole between SMMR and SSM/I.

We compute daily ice extent and then take monthly averages, rather than computing the ice extent from monthly averaged ice concentration fields, which avoids biases associated with the merging of temporal and spatial averages. We average the ice extent and ice area over all days in each month with data, with the exception of December 1987 and January 1988, when there is limited data as described above. These two months are filled using linear interpolation between the same month in the previous year and the following year. The result is a monthly time series of ice extent and ice area for each Bootstrap version in each hemisphere.

We also include analysis of an approximation to Version 1 ice extent and ice area in the Antarctic only, which we call "Version 1B". The Version 1B ice extent time series is identical to Version 2 except that $0.16 \times 10^6\,\mathrm{km}^2$ is removed from all months after December 1991. The Version 1B ice area time series is generated similarly, except that a somewhat somewhat smaller value of $0.12 \times 10^6\,\mathrm{km}^2$ is removed from all months after December 1991. In both cases, the size of the step function was chosen to match the Version 1 trend for the range of endpoints plotted in Fig. 1b (see Fig. S5c,g).

For the NASA Team algorithm, we use a time series of monthly-mean ice extent and ice area downloaded from the NSIDC "Sea Ice Index" archive (Fetterer et al., 2002). We interpolate over the months 12/1987 and 1/1988, as described above for the Bootstrap algorithm, and we add the area of the hole around the pole to the Arctic sea ice area.

The four time series of monthly-mean ice extent and ice area in each hemisphere all begin in November 1978, but they end at different times. The Bootstrap Version 1 data set ends in December 2004, the Bootstrap Version 1B and Version 2 data sets ends in December 2012, and the NASA Team data set ends in August 2013 (including near-real-time data during the months of 2013 because final NASA Team data was not yet available at the time of analysis).

S1.3 Documentation of update from Bootstrap Version 1 to Version 2

A separate satellite passive microwave data set is available from the Advanced Microwave Scanning Radiometer for the Earth Observing System (AMSR-E), which is flown on the NASA Aqua satellite. AMSR-E provided data from 19 June 2002 until 4 October 2011, when an antenna problem caused the sensor to stop operating. Compared to SSM/I, AMSR-E has finer spatial resolution and provides data over a wider range of microwave frequencies.

The Bootstrap algorithm was revised and a new version of the NASA Team algorithm (NASA Team 2) was created for use with the AMSR-E data (Comiso et al., 2003). Considering four years of overlap between AMSR-E and SSM/I (2002-2006), ice covers estimated with the Bootstrap algorithm from both satellites, as well as NASA Team SSM/I results, were all found to be in fairly good agreement overall for both hemispheres (Comiso and Parkinson, 2008; Parkinson and Comiso, 2008).

Nonetheless, Comiso and Nishio (2008) introduced an adjustment to the Bootstrap data set for consistency between the two instruments, after which Comiso and Nishio (2008) found that the 1978–2006 record that had AMSR-E data during 2002–2006 had a trend of $10.8 \times 10^3\,\mathrm{km}^2\,\mathrm{yr}^{-1}$, nearly identical to the 1978–2006 trend in the original SMMR and SSM/I Bootstrap data set which they found to be $10.9 \times 10^3\,\mathrm{km}^2\,\mathrm{yr}^{-1}$.

Other adjustments to the Bootstrap algorithm were also documented around this time. The Bootstrap algorithm formerly used only the 19V and 37V channels in the Antarctic, whereas it uses the 19V, 37V, and 37H channels in the Arctic where the fraction of first-year ice is smaller. The algorithm was updated to use the 19V, 37V, and 37H channels in the Antarctic, as in the Arctic, in order to remove a small negative bias identified in the ice concentration (Comiso, 2007).

After these changes were made to the Bootstrap algorithm, the entire data set was reprocessed and updated from Version 1 to Version 2 on the NSIDC website (Comiso, 2000).

We note that there appears to be some ambiguity in the Bootstrap data set version control. For example, the "Version History" in the NSIDC online documentation (Comiso, 2000) mentions the adjustment in Version 2 for consistency with AMSR-E but does not mention the change in input channels. However, the more extensive documentation linked from the website (Comiso, 2007), which does not explicitly mention version numbers, refers to the change in input parameters as "the biggest change in the revised version of the Bootstrap data set".

S2 Structure of trends in both hemispheres

Here we examine further details of the sea ice trends that are not included in the main paper. We examine ice extent as well as ice area. For comparison with the two Bootstrap versions, we consider ice cover estimated using the NASA Team algorithm. We also consider the ice extent and ice area from the same three data sets in the Arctic.

S2.1 Monthly ice extent and ice area

We focus on anomalies from the mean seasonal cycle in each record (Fig. S1). The difference between the two Bootstrap versions and the NASA Team ice extent is plotted in Fig. S2b,c in order to see whether it allows us to discern which of the two Bootstrap versions had a spurious jump in December 1991. These differences are too large and noisy to isolate any readily discernible change around December 1991. In Fig. S2c, however, there appears to be a rather subtle tendency for low values before December 1991 and high values afterwards, similar to Fig. S2a. This would imply an error in Version 2, but further statistical analyses would be required to determine whether this difference, which is largely masked by month-to-month variability, is statistically meaningful.

It should be noted that Figs. S2b,c display an apparent jump from high values before the 1987 sensor transition to low values afterwards, implying a possible difference between NASA Team and the two Bootstrap versions in the intercalibration across the transition from SMMR to SSM/I.

Similar to ice extent, the difference in ice area between Bootstrap Version 2 and Version 1 shows a clear transition in December 1991 (Fig. S2d). But for ice area, as for ice extent, the difference between each Bootstrap version and the NASA Team data is too large and variable to readily discern which Bootstrap data set experienced the spurious jump (Fig. S2e,f): there is no readily discernible step in December 1991 that stands out above the month-to-month variability. However, there appears to be a rather subtle transition from low to high values at the 1991 sensor transition in Fig. S2f, although more work would be needed to determine whether it is statistically meaningful.

Because similar algorithms are used in both hemispheres, we also consider ice extent and ice area anomalies in the Arctic (Fig. S3). A notable feature of the ice extent and ice area anomalies in all three data sets is the onset of large-amplitude low-frequency variability beginning in 2007 (Fig. S3b,d). This may be attributable to issues of coastline geometry causing the ice extent seasonal cycle amplitude to increase (Eisenman, 2010).

A number of changes in the Arctic sea ice extent data sets approximately coincide with sensor changes. A bias in the difference between the Bootstrap data sets appears to be introduced at the 1987 sensor change and then approximately compensated for at the 1992 sensor change (Fig. S4a). Similarly, a persistent offset between the NASA Team record and the two Bootstrap records appears to be introduced at the sensor change in 1987 (Figs. S4b,c). Furthermore, the NASA Team ice extent briefly drops considerably below both Bootstrap versions around the 1987 sensor change and briefly rises considerably above them around the 1995 sensor change, causing noticeable spikes in the comparison between NASA Team and either Bootstrap version that approximately coincide with the times of the sensor changes (Figs. S4b,c).

The Arctic sea ice area also shows a spike that approximately coincides with the 1987 sensor change (Figs. S4e,f). There appears to also be a rather subtle tendency for Bootstrap Version 2 to be higher than Version 1 after the 1992 sensor change (Fig. S4d).

Overall, we do not see a compelling indication in the Arctic ice extent or ice area data whether Bootstrap Version 1 or Version 2 is more likely to contain errors in both hemispheres.

S2.2 Ice extent and ice area trends

We examine the trend in the Bootstrap Version 1 and Version 2 data, as well as the NASA Team data, in both hemispheres. It is instructive to compare the differences between the data sets with the reported error bar on the trend, which provides an indication of the significance of the difference in trend between Version 1 and Version 2. Ice extent trends are often reported with error bars based on the 68% linear regression confidence interval using monthly data (e.g., Comiso and Steffen, 2001; Comiso, 2003; Comiso and Nishio, 2008; Comiso, 2010), which is an estimate of the error associated with natural variability about the trend. The IPCC AR4 and IPCC AR5 instead use a 90% linear regression confidence interval, with the IPCC AR4 using annual data and the IPCC AR5 using monthly data (see Appendix A1 of main text). Hence we plot both the 68% and 90% confidence intervals, as well as the 99% confidence interval, for monthly and annual data (Figs. S5-S8). We also compare trends in both Bootstrap data sets with the values reported in the two IPCC reports in Table S1.

In the Antarctic, the Bootstrap Version 2 ice extent trend is well outside the 90% confidence interval of the Bootstrap Version 1 trend and near the edge of the 99% confidence interval for all plotted record endpoints (Fig. S5b). Similar features apply to the trend in ice area: Bootstrap Version 2 is near the edge of the 99% confidence interval of Bootstrap Version 1 (Fig. S5f).

The trend in the Bootstrap Version 2 ice extent (Fig. S5a) agrees fairly closely with the NASA Team data (Fig. S5d), whereas Bootstrap Version 1 does not (Fig. S5b), implying that an error in the Bootstrap data set may have been corrected between Version 1 and Version 2. In contrast, however, the trend in NASA Team ice area (Fig. S5h) agrees closely with Bootstrap Version 1 (Fig. S5f) but not with Bootstrap Version 2 (Fig. S5e), implying instead that Version 2 introduced an error into the Bootstrap data set that did not exist in Version 1. This could be related to the previously discussed low bias in NASA Team ice concentration (e.g., Comiso et al., 1997), which could plausibly affect the ice area trend.

However, the comparison is reversed in the Arctic. The trend in Arctic sea ice area agrees closely between both Bootstrap versions and NASA Team, whereas the trend in Arctic sea ice extent differs substantially between each of the three records (Fig. S7). Interestingly, the trend in Bootstrap

Version 2 Arctic sea ice extent falls near the edge of the 99% regression confidence interval of the NASA Team trend (Fig. S7c): If both current data sets are seen as reliable estimates of the sea ice cover, then this indicates that the regression confidence interval substantially underestimates the uncertainty in the Arctic sea ice trend by failing to account for errors associated with the satellite retrieval algorithm.

In the Arctic, the trend in sea ice extent differs between Version 1 and Version 2 (Fig. S7), as in the Antarctic. However, in contrast to the Antarctic, this change is relatively small compared with the changes in the linear trend during the past decade associated with the actual acceleration of the ice retreat.

It is interesting in Fig. S7 that for ice extent and ice area in all the data sets, the trend appears to remain relatively constant before ∼2005, then to drop rapidly, and then to drop more slowly after ∼2007, although the extent to which these features are statistically meaningful is not investigated here.

The trends in both hemispheres using annual data (Figs. S6,S8) resemble the trends from monthly data (Figs. S5,S7), except that the error bars are typically approximately twice as large.

S2.3 Seasonal structure of trends

There is not a strong seasonal structure to the trend in the Antarctic sea ice cover in any of the data sets considered here (Fig. S9). Although the trend is larger in March/June than in September/December for many record endpoints in all three ice extent data sets, both Bootstrap Version 2 and NASA Team produce ice extent and ice area trends that are smallest in March for the most recent record endpoints. Other studies that have reported the trend to be largest in Austral summer have measured the trend in percent per decade, dividing the trend by the mean value for each month and thereby introducing a strong seasonality associated with the denominator (e.g., Turner and Overland, 2009).

The seasonal uniformity in the Antarctic is in contrast with the Arctic (Fig. S10), where the retreat is fastest in boreal late summer, a feature that has been attributed to the configuration of continents in the Arctic (Eisenman, 2010).

S2.4 Spatial structure of trends

The spatial structure of the trends in both Bootstrap versions is compared in Fig. S11. We consider the change between the late 1980s and the late 1990s in order to focus on the shift that occurred in December 1991 (Fig. 2). Both versions have nearly identical spatial patterns of the change for all seasons during this time period, and the first row of Fig. S11 is nearly indistinguishable from the second row. However, it is the relatively small difference between large regional expansions and contractions that give rise to the trend in total ice extent or ice area. Considering the difference between the two versions (lowest row of Fig. S11), Version 2 changes in a more positive way than Version 1 during this period in most locations and seasons. This difference is relatively uniform spatially and among seasons, in contrast with the strongly spatially-varied trend in each data set individually and consistent with a sensor intercalibration issue explaining the difference between the versions.

References

Cavalieri, D. J., Crawford, J. P., Drinkwater, M. R., Eppler, D. T., Farmer, L. D., Jentz, R. R., and Wackerman, C. C.: Aircraft active and passive microwave validation of sea ice concentration from the defense meteorological satellite program special sensor microwave imager, J. Geophys. Res., 96, 21 989–22 008, doi:10.1029/91JC02335, 1991.

Cavalieri, D. J., Parkinson, C. L., Gloersen, P., Comiso, J. C., and Zwally, H. J.: Deriving long-term time series of sea ice cover from satellite passive-microwave multisensor data sets, J. Geophys. Res., 104, 15 803–15 814, doi:10.1029/1999JC900081, 1999.

Comiso, J. C.: Bootstrap Sea Ice Concentrations from Nimbus-7 SMMR and DMSP SSM/I-SSMIS. Version 2, Updated 2012, National Snow and Ice Data Center, Boulder, CO, USA, available at: http://nsidc.org/data/nsidc-0079.html (last access: 30 September 2013), 2000.

Comiso, J. C.: Large scale characteristics and variability of the global sea ice cover, in: Sea Ice – An Introduction to its Physics, Biology, Chemistry and Geology, Blackwell Scientific Ltd., Oxford, UK, 112–142, 2003.

Comiso, J. C.: Enhanced Sea Ice Concentrations from Passive Microwave Data. National Snow and Ice Data Center, Boulder, CO, USA, available at: http://nsidc.org/data/docs/daac/nsidc0079_bootstrap_seaice/docs/Bootstrap_Algorithm_Revised07.pdf (last access: 30 September 2013), 2007.

Comiso, J. C.: Variability and trends of the global sea ice cover, in: Sea Ice, 2nd edn., Wiley-Blackwell, Oxford, UK, 205–246, 2010.

Comiso, J. C. and Nishio, F.: Trends in the sea ice cover using enhanced and compatible AMSR-E, SSM/I, and SMMR data, J. Geophys. Res., 113, C02S07, doi:10.1029/2007JC004257, 2008.

Comiso, J. C. and Parkinson, C. L.: Arctic sea ice parameters from AMSR-E data using two techniques and comparisons with sea ice from SSM/I, J. Geophys. Res., 113, C02S05, doi:10.1029/2007JC004255, 2008.

Comiso, J. C. and Steffen, K.: Studies of Antarctic sea ice concentrations from satellite data and their applications, J. Geophys. Res., 106, 31361–31385, doi:10.1029/2001JC000823, 2001.

Comiso, J. C., Cavalieri, D. J., Parkinson, C. L., and Gloersen, P.: Passive microwave algorithms for sea ice concentration: A comparison of two techniques, Remote Sens. Environ., 60, 357–384, 1997.

Comiso, J. C., Cavalieri, D. J., and Markus, T.: Sea ice concentration, ice temperature, and snow depth using AMSR-E data, IEEE Transactions On Geoscience Remote Sensing, 41, 243–252, doi:10.1109/TGRS.2002.808317, 2003.

Eisenman, I.: Geographic muting of changes in the Arctic sea ice cover, Geophys. Res. Lett., 37, L16 501, doi:10.1029/2010GL043741, 2010.

Fetterer, F., Knowles, K., Meier, W., and Savoie, M.: Sea ice index, Updated 2012, National Snow and Ice Data Center, Boulder, CO, USA, available at: http://nsidc.org/data/g02135.html (last access: 1 July 2013), 2002.

IPCC: Climate Change 2007: The Physical Science Basis. Contribution of Working Group I to the Fourth Assessment Report of the Intergovernmental Panel on Climate Change, edited by: Solomon, S., Qin, D., Manning, M., Chen, Z., Marquis, M., Averyt, K. B., Tignor, M., and Miller, H. L., Cambridge University Press, Cambridge, United Kingdom and New York, NY, USA, 2007.

Parkinson, C. L. and Comiso, J. C.: Antarctic sea ice parameters from AMSR-E data using two techniques and comparisons with sea ice from SSM/I, J. Geophys. Res., 113, C02S06, doi:10.1029/2007JC004253, 2008.

Screen, J. A.: Sudden increase in Antarctic sea ice: Fact or artifact?, Geophys. Res. Lett., 38, L13 702, doi:10.1029/2011GL047553, 2011.

Turner, J. and Overland, J.: Contrasting climate change in the two polar regions, Polar Res., 28, 146–164, doi:10.1111/j.1751-8369.2009.00128.x, 2009.

Table S1. Trends for different time periods and data sets, including 90% regression confidence interval error bars, in units of $10^3\,\mathrm{km}^2\,\mathrm{yr}^{-1}$. Annual trends are calculated using January–December averages for each year. The slight differences between trends reported in the IPCC reports and those computed here with the matching Bootstrap version are expected to arise due to issues including rounding errors and slight differences in the data sets and methodology such as how missing data is treated and how ice extent is calculated from the gridded ice concentration fields.

	11/1978–12/2005 monthly	1979–2005 annual	11/1978–12/2012 monthly	1979–2012 annual
IPCC AR4		5.6 ± 9.2		
Bootstrap v1B	4.9 ± 4.5	5.2 ± 8.0	10.3 ± 3.5	10.5 ± 6.7
IPCC AR5			16.5 ± 3.5	
Bootstrap v2	13.7 ± 4.5	14.1 ± 8.2	16.9 ± 3.5	17.2 ± 6.6

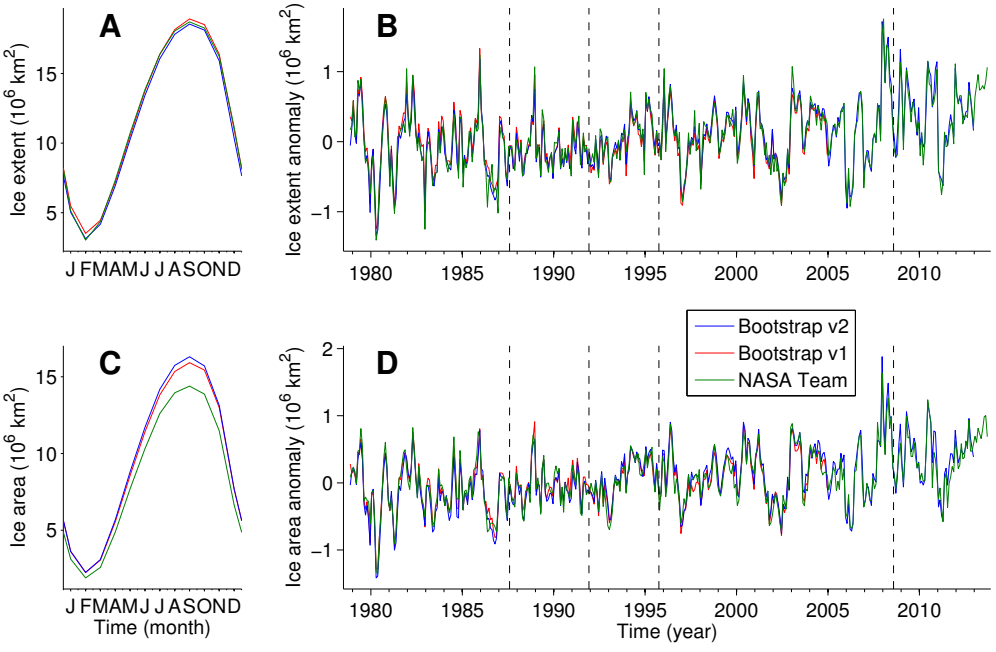

Fig. S1. (A) Mean seasonal cycle of Antarctic sea ice extent during 1979–2004 and (B) time series of monthly-mean anomalies from the mean seasonal cycle for both versions of the Bootstrap data as well as the NASA Team data. (C)-(D) Same, but for ice area rather than ice extent. Transitions between sensors are indicated by vertical dashed lines (see Sect. S1.1).

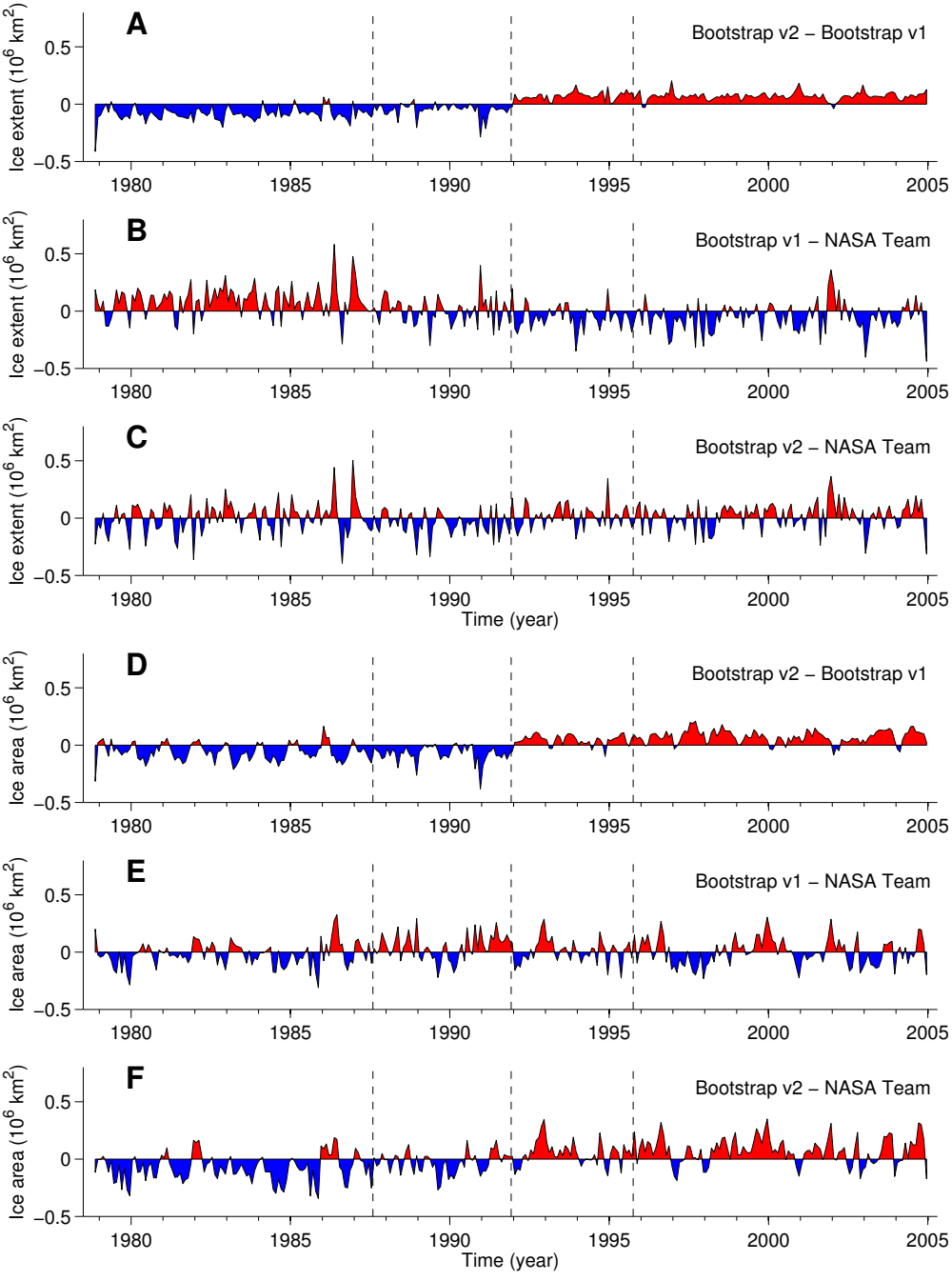

Fig. S2. Antarctic sea ice anomalies from the 1979–2004 mean seasonal cycle. (A-C) Difference between monthly-mean Antarctic sea ice extents computed using Bootstrap Version 1, Bootstrap Version 2, and NASA Team data sets. Data sets are indicated in the top right corner of each panel. Panel A is equivalent to Fig. 2. (D-F) Same, but for ice area rather than ice extent. Transitions between sensors are indicated by vertical dashed lines (see Sect. S1.1). The plotted time interval is the period during which Bootstrap Version 1 data is available.

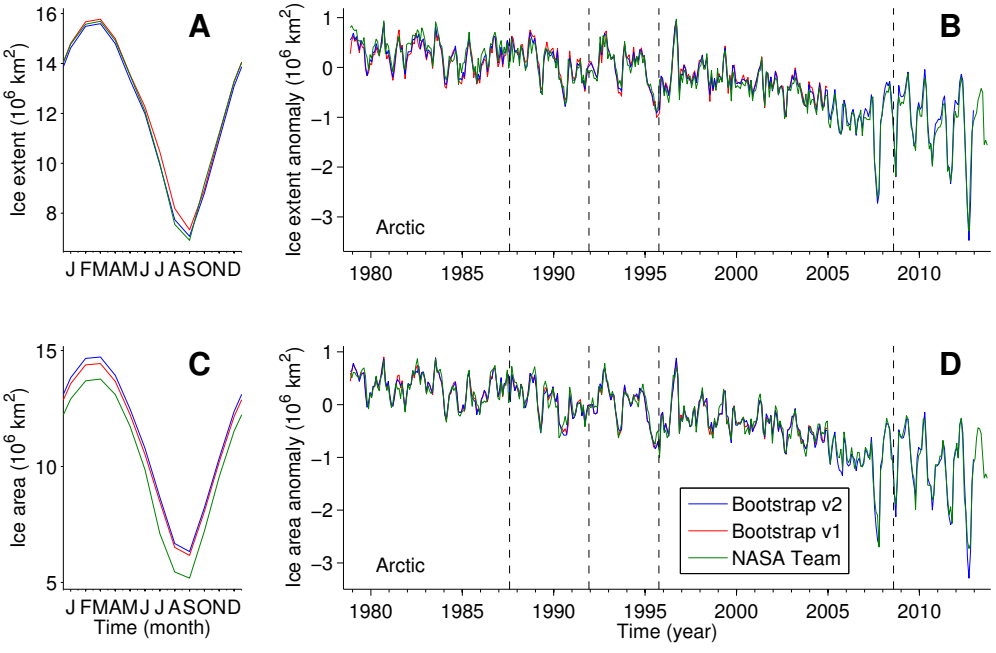

Fig. S3. As in Fig. S1, but for the Arctic.

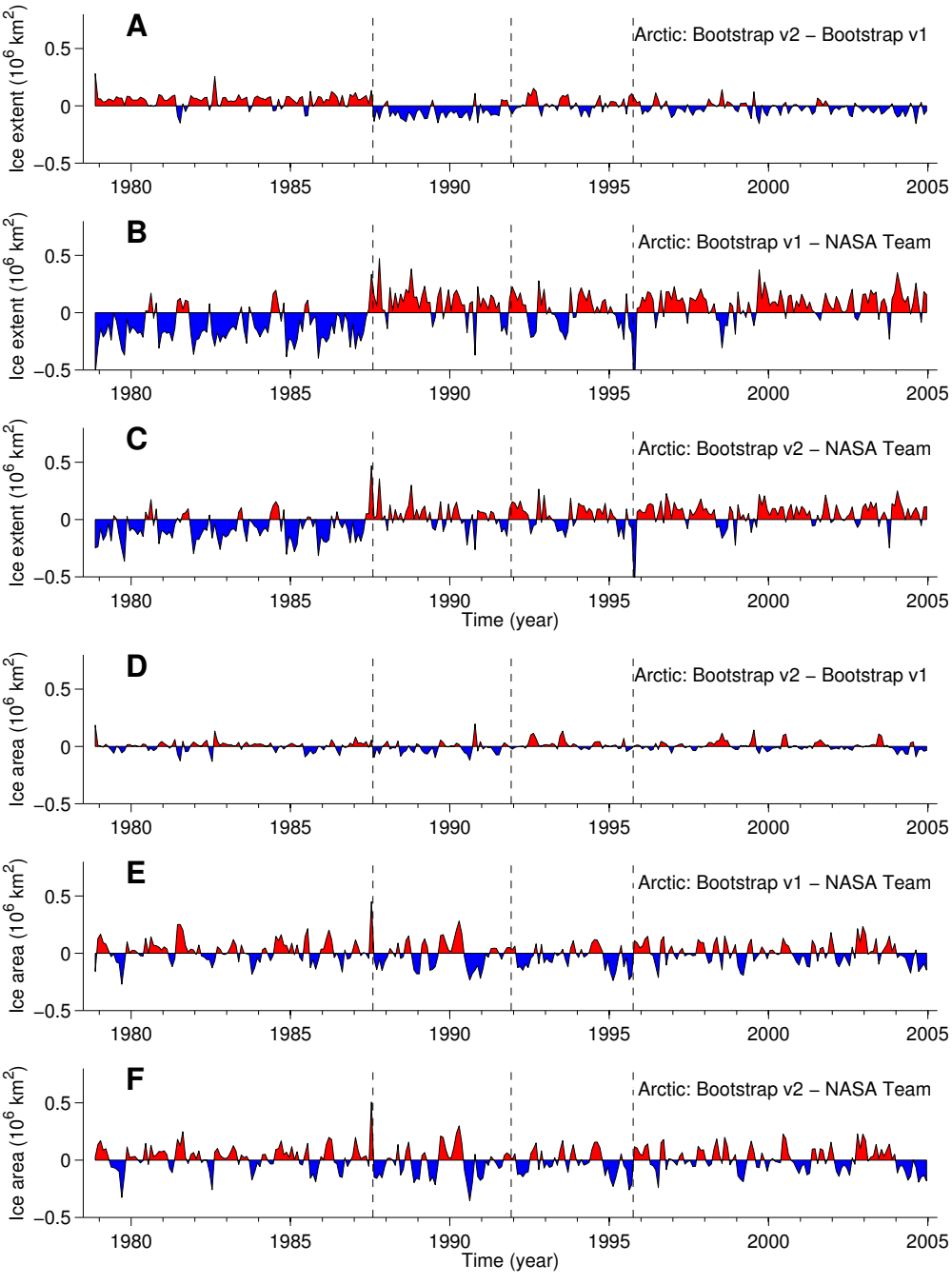

Fig. S4. As in Fig. S2, but for the Arctic.

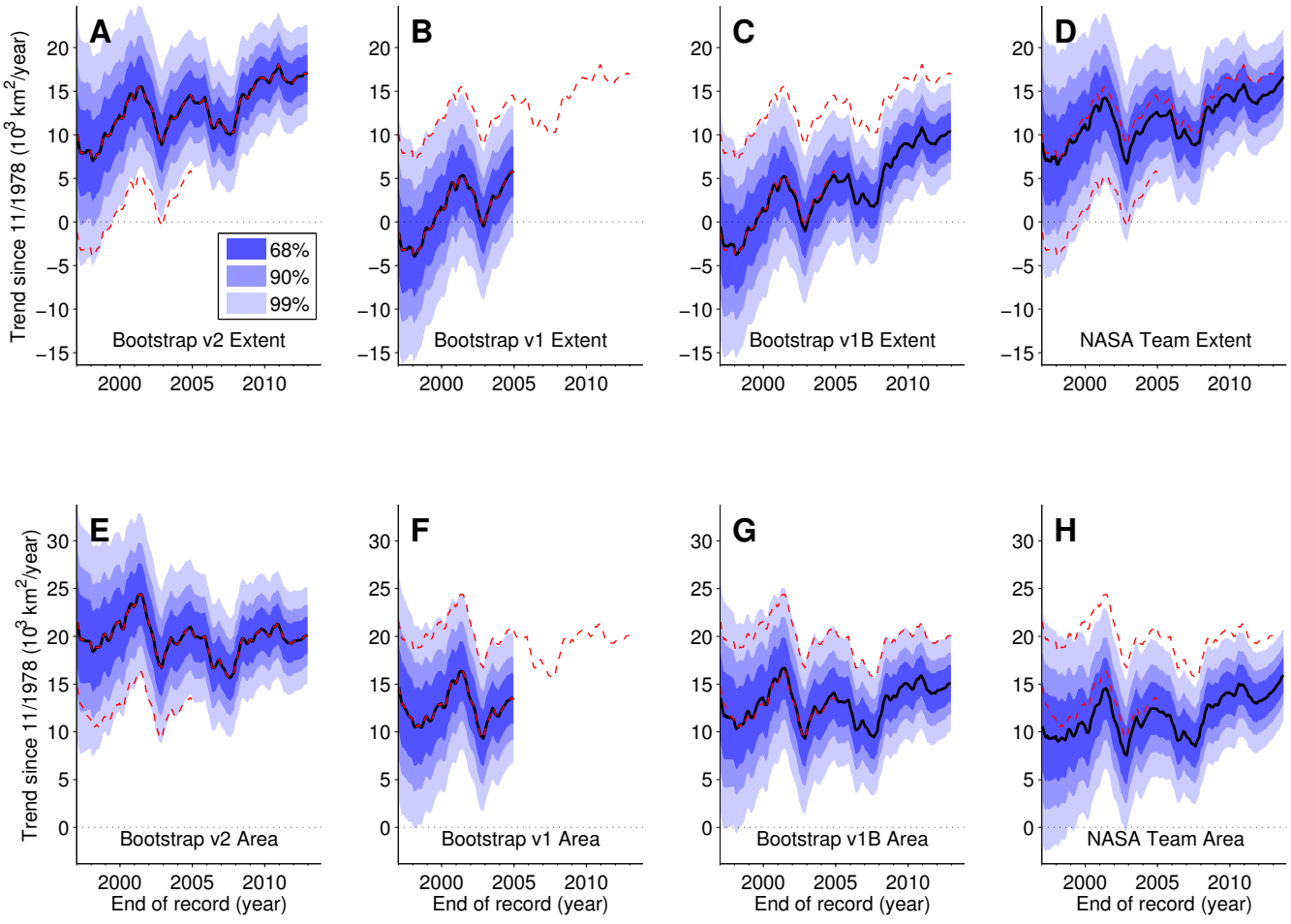

Fig. S5. Trends in Antarctic sea ice extent (top) and area (bottom) using Version 1, Version 1B, and Version 2 of the Bootstrap data set, as well as the NASA Team data set, for a range of record endpoints. Shades of blue indicate the 68% regression confidence interval (which is often used to represent the trend error bar in published studies), the 90% confidence interval (which is used to represent the error bar in the IPCC reports), and the 99% confidence interval. The trends computed using Version 1 and Version 2 of the Bootstrap data set (red dashed lines) are repeated across each row for comparison.

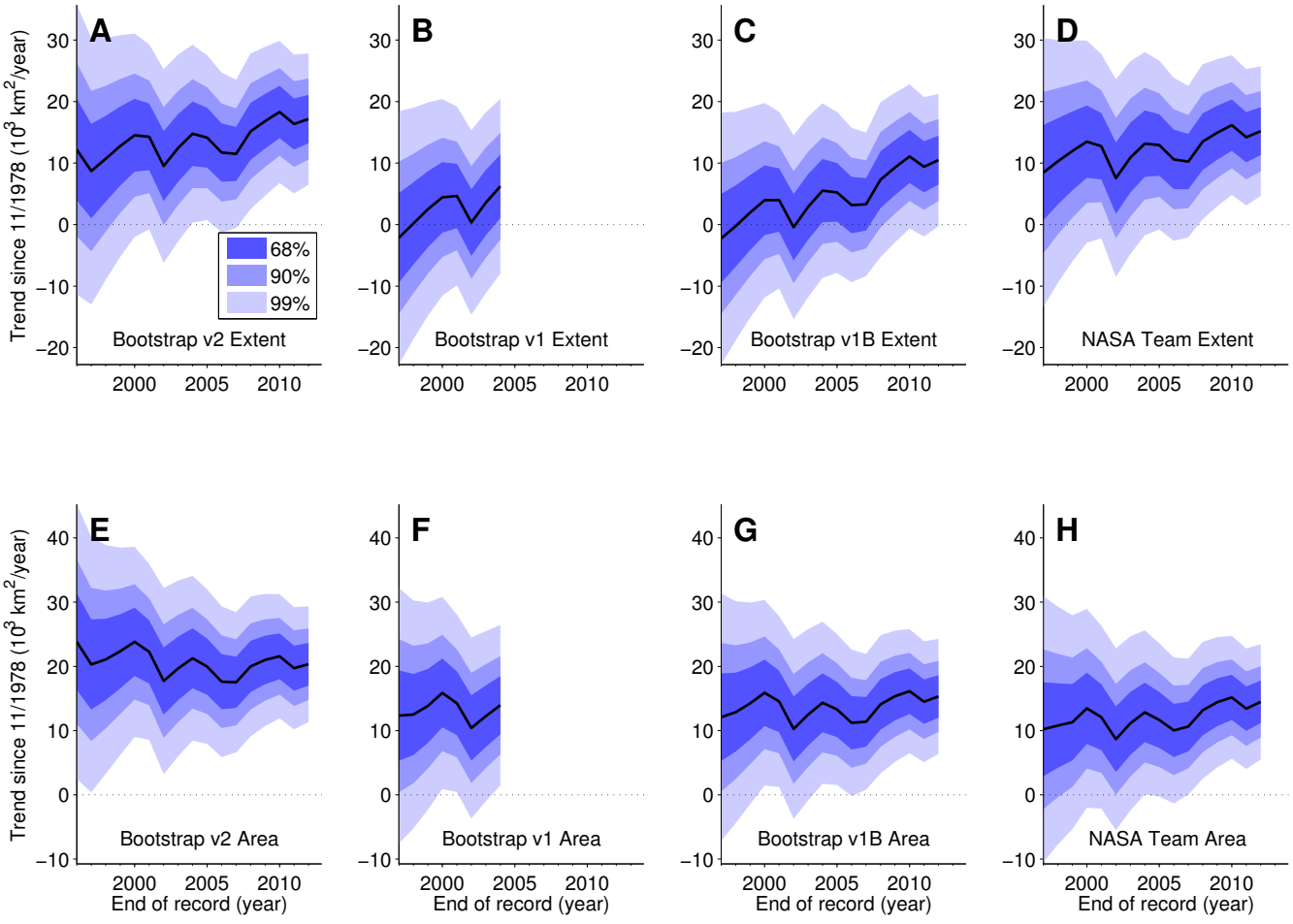

Fig. S6. As in Fig. S5, but using annual data. Note that the horizontal axis range is shifted compared with Fig. S4. This is because, for example, the trend in the data set that goes to the end of 2005 is plotted above the 2005 tick in this figure but above December 2005 (near the 2006 tick) in Fig. S4.

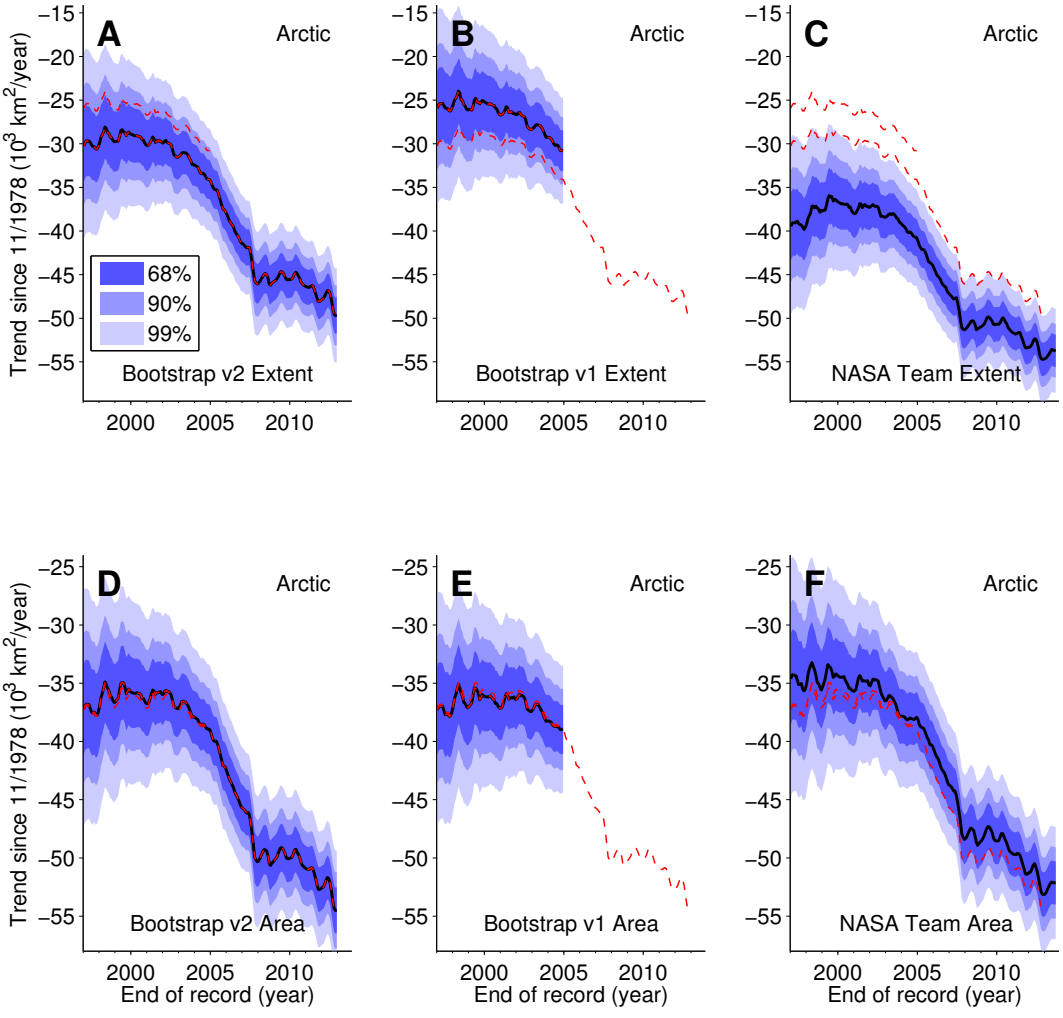

Fig. S7. As in Fig. S5, but for the Arctic.

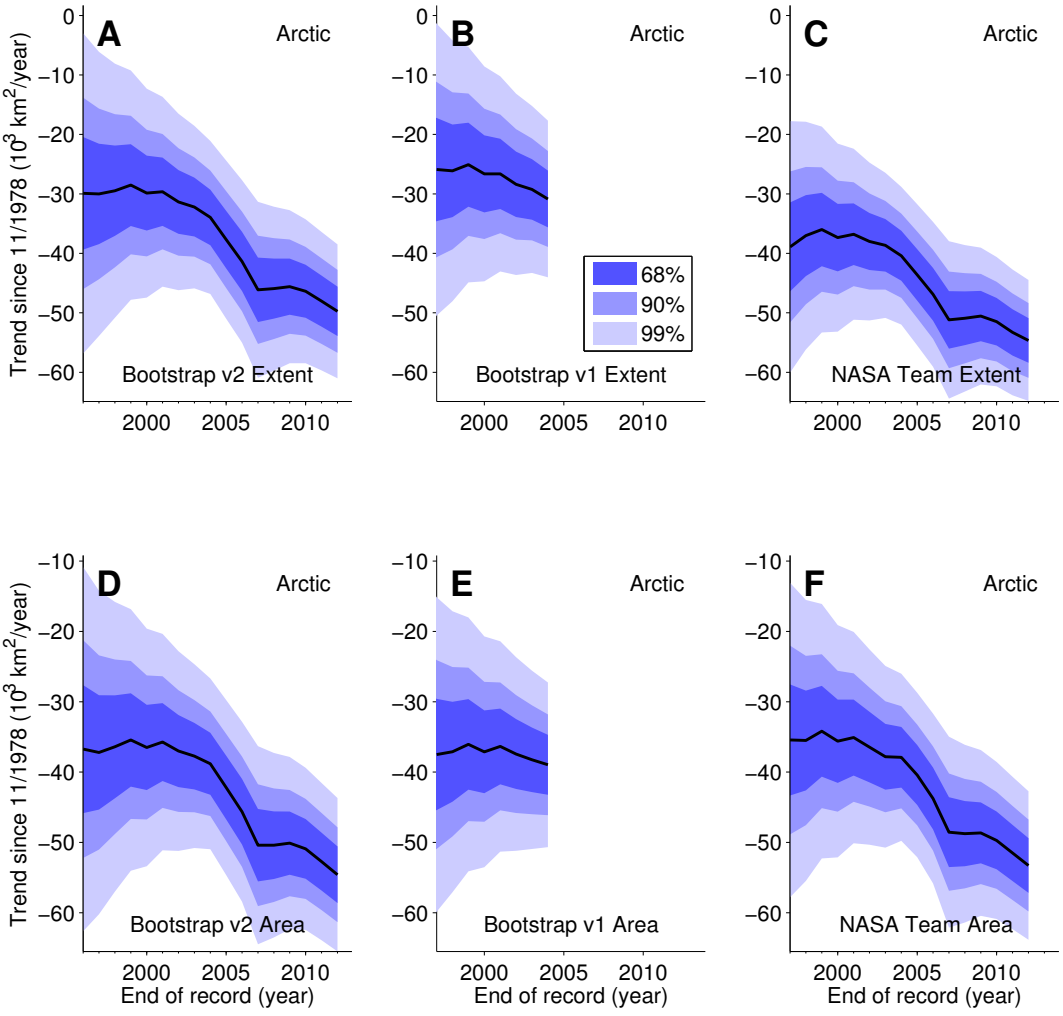

Fig. S8. As in Fig. S6, but for the Arctic.

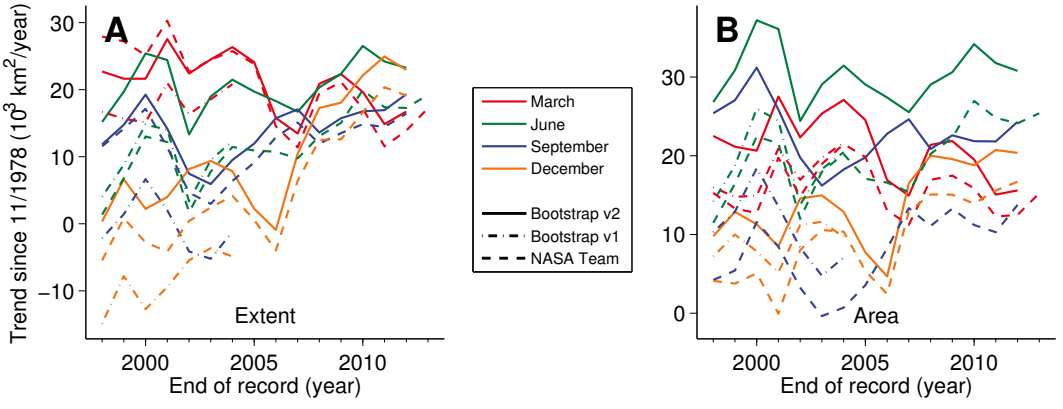

Fig. S9. Seasonal structure of trends in Antarctic (A) ice extent and (B) ice area. Here the trends are computed using only every March (red), June (green), September (blue), or December (orange) for a range of record endpoints. Results are plotted for Version 2 of the Bootstrap data set (solid), Version 1 of the Bootstrap data set (dot-dash), and the NASA Team data set (dash).

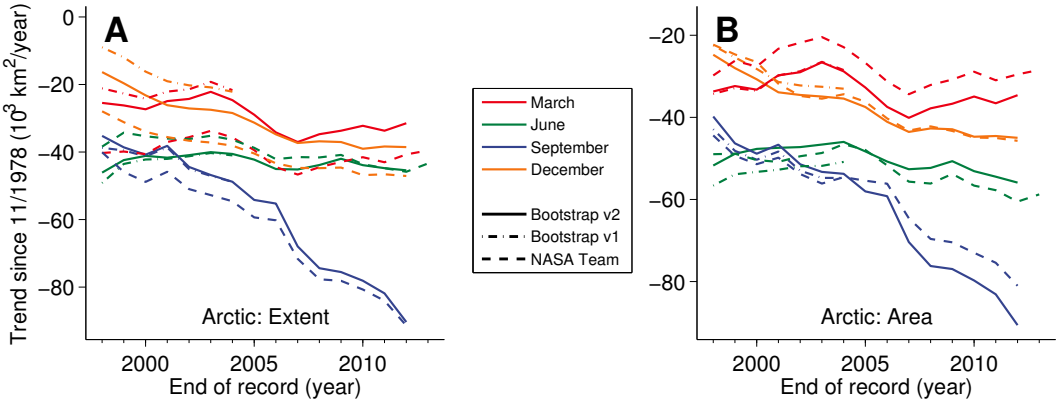

Fig. S10. As in Fig. S9, but for the Arctic.

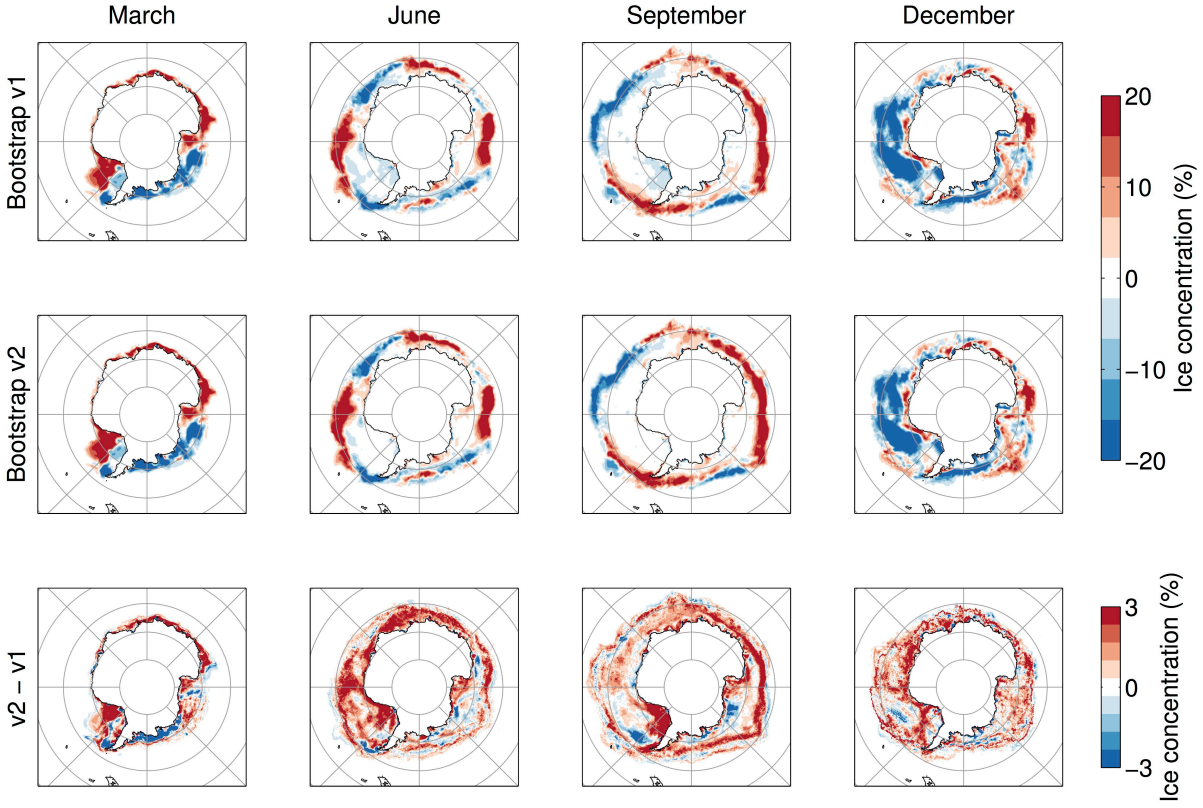

Fig. S11. Spatial structure of changes in Antarctic sea ice cover. (Top row) Change between late 1980s and late 1990s, calculated as the mean during 1985–1989 subtracted from the mean during 1995–1999, in the Bootstrap Version 1 data set. (Middle row) Same, but for the Bootstrap Version 2 data set. (Bottom row) Difference between Bootstrap versions, calculated as Version 2 minus Version 1. Each column represents a different month.